International Journal of Nanoelectronics and Materials
Volume 13, No. 2, Apr 2020 [323-340]

Optimizing Plasmonic Characteristics of Ag-AuNPs/Nanohillocks Si Heterostructures for Efficient SERS Performance

Alwan M. Alwan[1], Mohammed S. Mohammed[1] and Russul M. Shehab[1*]

[1]*Department of Applied Sciences, University of Technology, Baghdad-Iraq.*

Received 7 November 2019, Revised 29 December 2019, Accepted 6 February 2020

ABSTRACT

Tunable bimetallic Ag-Au nanoparticles (Ag-AuNPs) and hot spot regions were created through the reduction of Ag-Au ions onto nanohillock silicon surfaces. A set of as-prepared textured silicon substrates with different nanohillock topographies was synthesised by a wet potassium hydroxide (KOH) chemical etching process on crystalline silicon for incubation times from 4 to 10 min. These structures were explored as a substrate for optimizing the plasmonic characteristics of Ag-AuNPs/nanohillocks Si surface-enhanced Raman scattering (SERS) heterostructures. The goal of this paper is to create sufficient SERS heterostructures with a high enhancement and exceptional reproducibility. The nanohillock Si substrate was employed to create nearly homogeneously distributed Ag-AuNPs and hot spot regions with extraordinary specific surface area (S.S.A.) values. Plasmonic characteristics of the created Ag-AuNPs were investigated and analysed based on the surface features of the substrate via atomic force microscopy (AFM), field emission scanning electron microscopy (FE-SEM), X-ray diffraction spectroscopy (XRD), energy-dispersive X-ray spectroscopy (EDS) and Raman measurements. Tunable Ag-AuNPs sizes and hot spot regions were synthesized by controlling the incubation time of the wet KOH chemical etching process. The density and size distribution, and hence the plasmonic characteristics of the Ag-AuNPs and hot spot regions, were improved significantly with increasing surface roughness and average hillock height of the substrate and specific surface area of the Ag-AuNPs. A high enhancement factor of 3.7×10^{13} with a minimum reproducibility deviation of about 4% was attained in 10^{-14} M rhodamine 6G dye for an 8 min etching incubation time.

Keywords: Nanohillocks Silicon, KOH Chemical Etching, SERS; Plasmonic Characteristic, Ag-AuNPs.

1. INTRODUCTION

In many areas of chemistry and biology, surface-enhanced Raman scattering (SERS) has played a critical role in a variety of discoveries [1]. The performance of SERS heterostructures is strongly related to the microstructures of the SERS substrates and the density, uniformity and sizes of plasmonic nanostructures, as well as the hot spot regions, which all contribute to determining the enhancement factors and the reproducibility [2, 3]. When the target molecules lie within plasmonic hot spots, SERS signals can increase by 10^{10}–10^{12} times [4]. The two critical factors governing SERS performance are the type of plasmonic nanostructure material and the structure of the substrate. Monometallic nanoparticles composed of gold, silver, palladium and copper have been used as plasmonic nanostructures for creating SERS heterostructures [5,6]. Bimetallic nanoparticles are nano-scale materials that may be alloyed in the nanoscale regime to

*Corresponding Author: *russullaser@yahoo.com*

enhance their SERS properties. Bimetallic nanoparticles have attracted significant attention because of their unique properties that differ from those of monometallic nanoparticles [7].

The Raman intensities from SERS heterostructures with silver nanoparticles (AgNPs) exhibit larger enhancements than those of gold nanoparticles (AuNPs) because of their powerful interparticle close-field conjunction effects and more acute plasmonic peaks, but they suffer from rapid sulfuration and surface oxidation processes. The alloying of Ag-Au bimetallic nanoparticles represents a way to overcome these disadvantages [8, 9].

Texturing of silicon substrates through anisotropic wet etching of Si in a KOH solution is a low cost, simple and effective process for controlling the topographical properties of Si substrates for several applications, such as ultra-fast capacitors and efficient solar cells [10,11]. Anisotropic etching is an effective wet texturing process because of the low occurrence of defects and surface states [12-14]. Anisotropy and the formation of pyramidal or hillock structures occur because the elimination of surface atoms is a site-dependent method in the microscopic regime [15]. A SERS-active substrate based on porous silicon was studied previously by [2]. The performance showed a high divergence in both the reproducibility and enhancement factor (EF) due to the nonuniformity of the porous layer.

The aim of this work is to develop and optimize the plasmonic characteristics of Ag-AuNPs/nanohillocks Si SERS heterostructures by controlling the sizes of the Ag-AuNPs and hot spot regions via the KOH incubation time.

2. MATERIAL AND METHODS

2.1 Chemical Materials

A (2 M) KOH solution, 0.001 M of high purity $HAuCl_4$ (99.98%) and $AgNO_3$ (Aldrich, 99.99%) was prepared by dissolving in Millipore H_2O according to the formula found in [9]. Rhodamine 6G (R6G) dye was employed as a probe molecule for investigating SERS efficiency.

2.2 Fabrication of Ag-AuNPs/Nanohillocks Si SERS Heterostructures

Two-sided polished crystalline silicon with (100) orientation and a resistivity of about 100 Ω.cm was ultrasonically washed for 15 minutes at room temperature with isopropyl alcohol and then chemically etched with a 2 M KOH solution to fabricate the nanohillock Si substrate. Different topographies of nanohillock Si surfaces were utilized by incubating the Si wafer in the KOH solution for incubation times of 4, 6, 8 and 10 minutes at room temperature. Tunable bimetallic Ag-AuNP sizes and hot spot regions were created through the Ag-Au ion reduction process on nanohillock Si surfaces by immersing textured silicon substrates in 5×10^{-3} M $AgNO_3$ and $HAuCl_4$ with equal mixing volumes for a period of 2.5 minutes. The Ag^{+1} and Au^{+3} reduction reaction involves the hydrogenated bonds, $Si\text{-}H_x$, of the textured silicon surface, as is expressed by [3,8,9] and presented in the following equations:

$$Au^{+3} + 3e^- \rightarrow Au \quad (1)$$

$$Ag^{+1} + e^- \rightarrow Ag \quad (2)$$

Figure 1 shows a schematic representation of the formation of Ag-AuNPs/nanohillocks on Si SERS heterostructures.

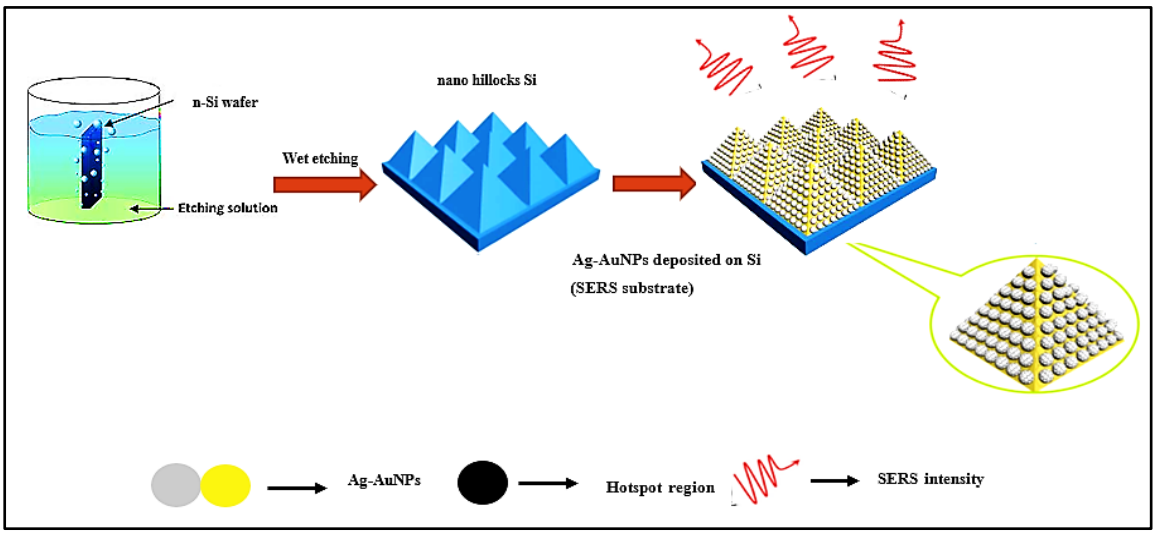

Figure 1. Schematic representation of formation Ag-AuNPs/nano hillocks Si SERS heterostructures.

2.3 Characterization of Ag-AuNPs/nanohillocks Si SERS heterostructures

Structural characteristics of the formed heterostructures were investigated and analysed based on the surface features of the Si nanohillocks via a TESCAN MIRA3 field emission scanning electron microscope (FE-SEM), a Bruker Multimode-8 atomic force microscope (AFM), a Shimadzu XRD-6000 X-ray diffraction (XRD) device, and energy dispersive X-ray spectroscopy (EDS). The sizes of the Ag-AuNPs were evaluated using ImageJ Type 8. Lastly, the SERS performance of the Ag-AuNPs/nanohillock Si SERS heterostructures in detecting R6G was carried out at dye concentrations of 10^{-8}, 10^{-10}, 10^{-12} and 10^{-14} M using a HoribaHR Evolution 800 Raman microscope system with a laser wavelength of 532 nm, laser power of about 30 mW and a laser spot diameter of about 0.1 μm. All the data were measured with a 10 seconds integration time.

3. RESULTS AND DISCUSSION

3.1 Topographical Features of As-Prepared Textured Si Substrates

The textured silicon samples displayed a darker and non-specular surface. Figure 2 depicts the AFM images of KOH-incubated Si surfaces etched with various incubation times. The AFM images of the textured silicon substrate display the typical surface topography of the etched silicon, which consists of interconnected Si nanohillocks. The creation of the hillock-like form may be attributed to the process of the anisotropic etching of crystalline Si in the KOH solution [16]. It is easily seen that the average height of the nanohillocks and the surface roughness vary with the incubation time. This textured silicon layer can efficiently increase the SERS sensitivity and is favourable for the creation of uniform Ag-AuNPs. For an incubation time of 4 minutes, the hillock-like structures seem dispersed on the Si surfaces. The growth in the volume of the hillock-like structures after a 6 minutes incubation leads to a heterogeneous volume distribution. After an incubation time of 8 minutes, large hillocks can be observed. Ultimately, these hillocks form a homogeneous and complete surface coverage after incubating the sample for 10 minutes. To analyse the topographical features of the textured silicon, three different criteria were taken into account. Figure 3 illustrates the measured criteria of the textured silicon, which were surface roughness (S_a), surface skewness (S_{ak}) and average hillock height as a function of incubation time.

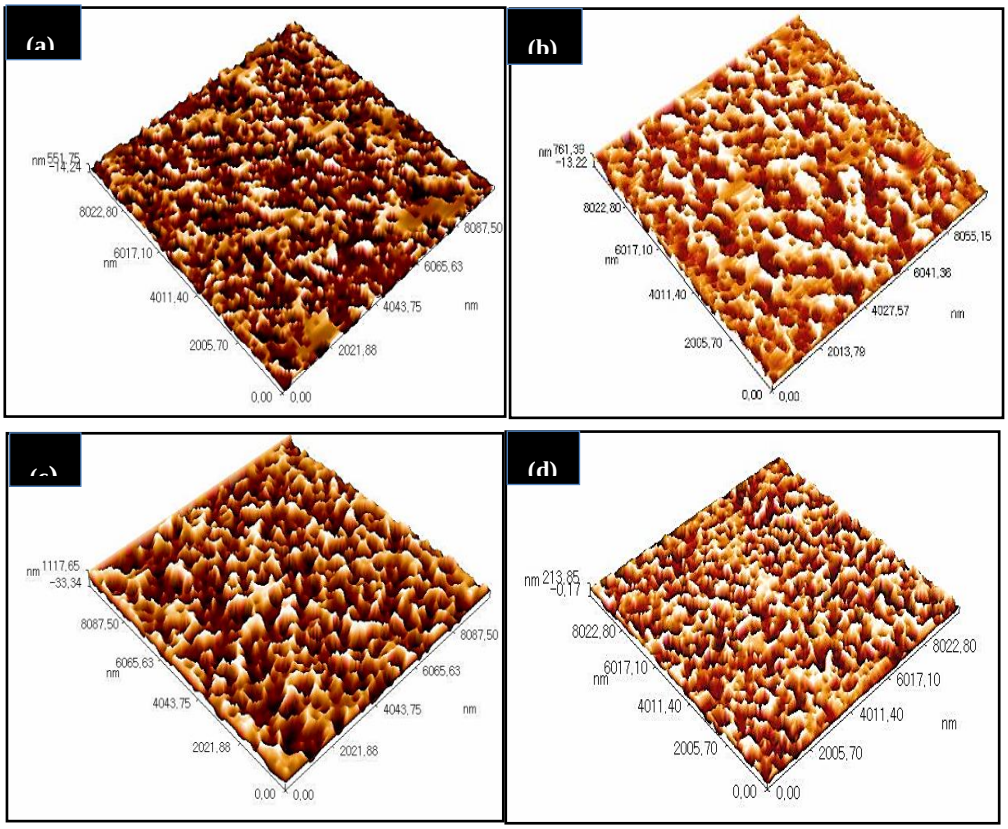

Figure 2. AFM images of as-prepared textured silicon substrates at different incubation times of (a) 4 minutes, (b) 6 minutes, (c) 8 minutes and (d) 10 minutes.

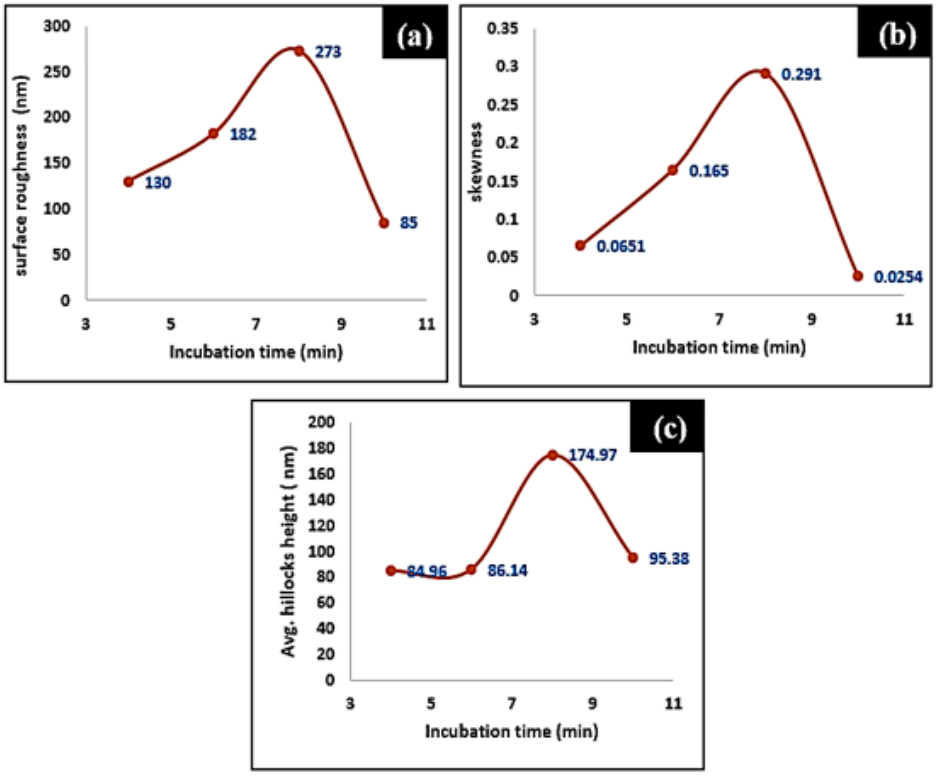

Figure 3. (a) Surface roughness Sa, (b) Surface skewness Sak, and (c) Average hillock height versus incubation time.

The first criterion of textured silicon is the surface roughness at an incubation time of 4 minutes, S_a=130 nm. Increasing the incubation time to 6 minutes leads to an increase in the value of S_a to 182 nm. At 8 minutes, the S_a increases to 273 nm, becoming more than twice its value at 4 minutes. So, Increasing the incubation time lead to increase S_a and hence improve the nucleation sites (Si-H) bound within the surface. Ultimately, at 10 minutes, this reflects the piecemeal growth of the hillock density, which achieves homogeneous and complete coverage at the surface that is led to reduce the surface roughness. For this incubation time, the S_a decreases to 82 nm as illustrated in Table (1).

The second criterion considered for the textured Si is skewness. It is beneficial to depict the interface morphology as the measurement of the reduction of distribution symmetry about the mean height. The development of the empirical time evolution of S_{ak} is illustrated in Figure 4(b). At an incubation time of 4 minutes, the skewness value is very low, up to 0.0651. S_{ak} undergoes a huge growth up to 0.165 at 6 minutes, which is related to the emergence of slightly larger hillocks. Subsequently, at 8 minutes, S_{ak} increases again because the surface is not yet entirely covered by the hillocks. Ultimately, at an incubation time of 10 minutes, when the Si surface is entirely covered with hillock structures, the skewness goes back to 0.0254. The hillocks size was influenced by the availability of the Si-H within the developed region, as the density of these sites decreased. This will be led to an increase in the sizes of the hillocks and decrease the roughness.

The third criterion for characterizing the Si surfaces is average hillock height. This is analysed to easily ascertain the height of the hillocks deposited on the Si. The average hillock height is related to the surface roughness, and a high average hillock height was obtained when the surface roughness was high. Figure 4(c) displays the experimental time evolution of the average hillock height. At an incubation time of 4 minutes, the average hillock height is very low, at 84.96 nm. It undergoes an increase up to 86.14 nm at 6 minutes, which correlates with increased surface roughness. Afterwards, at 8 minutes, the average hillock height is 174.97 nm. This large increase is due to the surface having a high roughness. Finally, at an incubation time of 10 minutes, the hillock density increased, and the surface was completely covered by the hillocks. At this point, the average hillock height returns to 95.38 nm.

Topographical features of the textured silicon are illustrated in Table (1). The textured silicone layer can efficiently increase the SERS sensitivity and is favourable for the uniform synthesis of a high density of small-sized Ag-AuNPs and, thus, tuneable bimetallic nanoparticle hot spot regions.

Table 1 Topographical features of textured Si substrates

Incubation time(min)	Surface roughness S_a(nm)	Skewness S_{ak}	Avg hillocks height(nm)
4	130	0.0651	84.96
6	182	0.165	86.14
8	273	0.291	174.97
10	82	0.0254	95.38

3.2 Structural Characteristics of Ag-Aunps/Nanohillocks Si SERS Heterostructures

Based on the results of topographical features of textured silicon (S_a, $S_{ak,}$ and average hillock height) of the as-prepared textured silicon substrates, the plasmonic characteristics of the Ag-AuNP heterostructures were studied. The uniformity of the heterostructures and their SERS performance were further analysed as a function of the structural characteristics of the synthesized Ag-AuNPs deposited over the Si nanohillock layer. Figure 4(a) presents the AFM image of bimetallic nanoparticles over the nanohillock Si layer of the substrate for the 8 minutes

incubation time, which provided the best texturing criteria. This textured silicon layer can efficiently improve the SERS sensitivity of the heterostructures due to the high density of deposited small-diameter Ag-AuNPs, which were about 91.69 nm in size, as depicted in Figure 4(b).

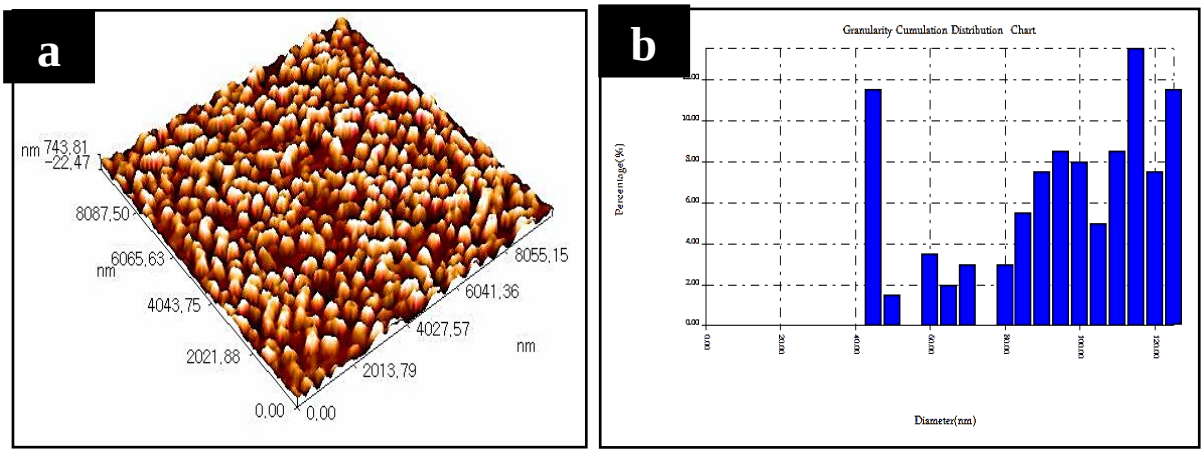

Figure 4. (a) AFM image of the textured Si substrate after deposition of Ag-AuNPs and (b) Mean diameter of Ag-AuNPs of the substrate for 8 minutes incubation time.

Figure 5(a-d) presents FE-SEM images of the textured Si substrates with incubation times of 4, 6, 8 and 10 minutes, respectively, after the deposition of the Ag-AuNPs. From these images, one can observe that the Ag-AuNPs consists of aggregates of semi-spherical metal nanoparticles on the textured Si with different sizes and different degrees of uniformity. The size difference of the Ag-AuNPs with increasing incubation time can be attributed to the aggregation process of the nanoparticles during the ion reduction method via the hydrogenated bonds of the Si nanohillocks [17,18]. Small size and a high degree of spatial uniformity of Ag-AuNPs over the textured Si surface is observed, and small nano-gap hot spots among the Ag-AuNPs can be easily recognized for the case of the 8 minutes incubation time. Meanwhile, for the incubation times of 4 and 6 minutes, the area is covered by larger Ag-AuNPs and nano-gaps, and the Ag-AuNPs/nanohillocks Si order is in one layer. With a longer incubation time of 10 minutes, the Ag-AuNPs were closely aggregated into groups of multi-Ag-AuNPs with a decreased density of nano-gaps. These bimetallic Ag-AuNPs entirely covered the nanohillock Si surface. This behaviour is more useful for improving the plasmonic enhancement of the hot spot regions and hence the performance of the heterostructures.

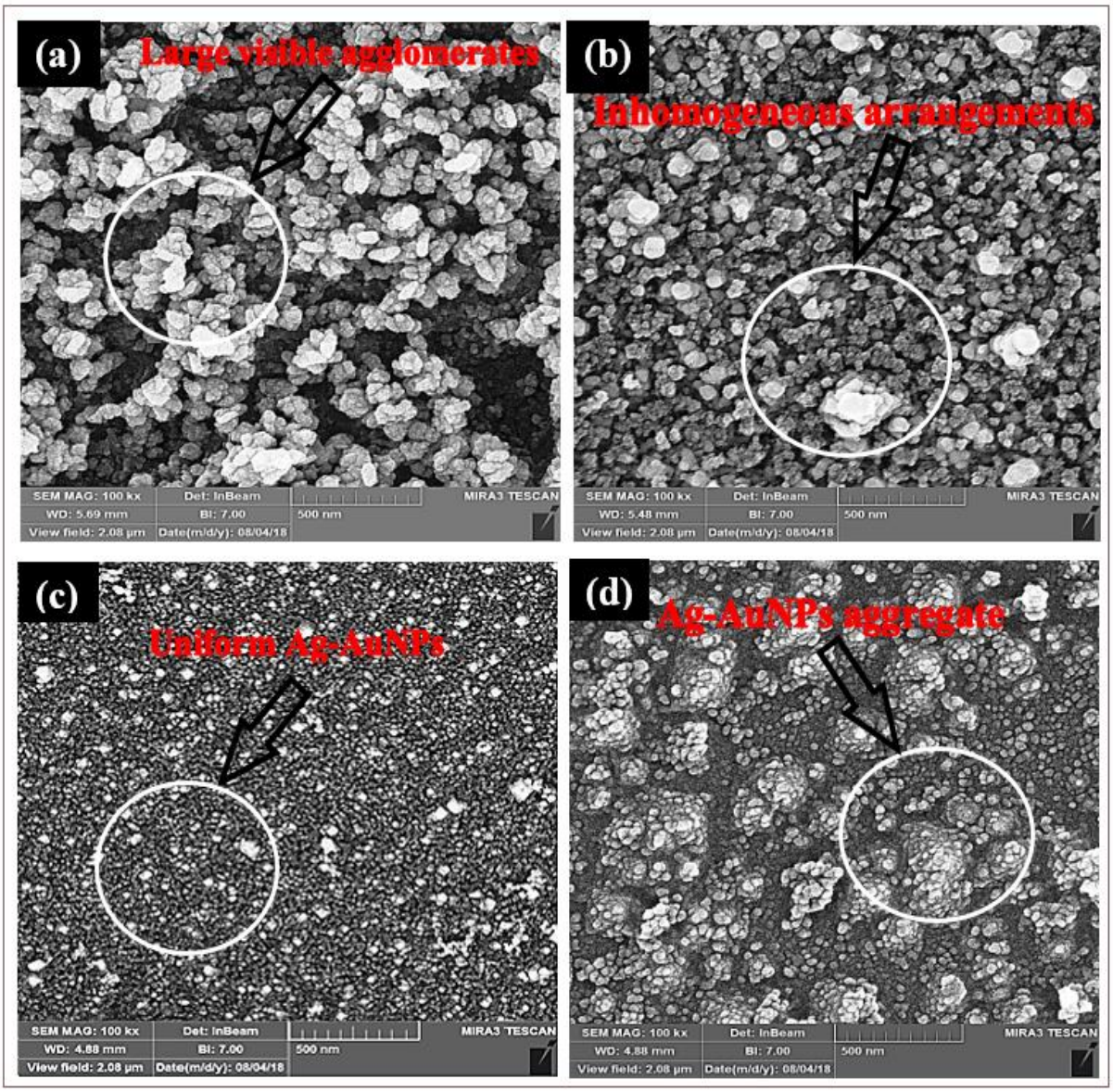

Figure 5. FE-SEM image textured Si substrate after deposition of Ag-AuNPs at different incubation times of (a) 4 minutes, (b) 6 minutes, (c) 8 minutes and (d) 10 minutes.

The histograms of the resulting nano-gaps (hot spot regions) amongst distributions of Ag-AuNPs are illustrated in Figure (6). According to these values, one can expect that the Raman intensity of Ag-AuNPs/nanohillocks Si heterostructures created by an 8 minutes incubation will have a larger value compared with the other incubation times studied, as shown in Table (2).

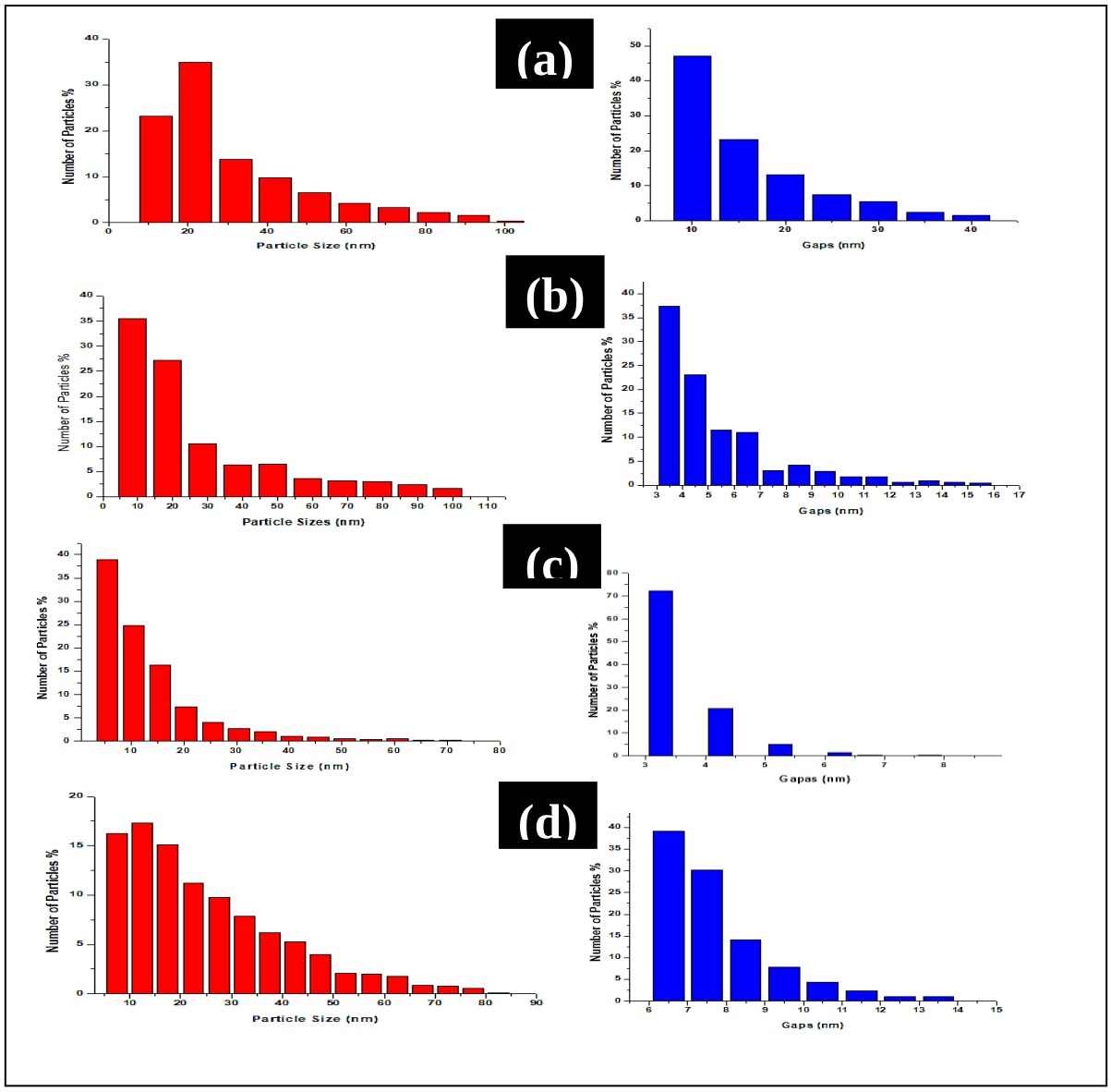

Figure 6. Histograms of the particle size distribution of Ag-AuNPs and hot spot sizes at incubation time (a) 4 minutes, (b) 6 minutes, (c) 8 minutes, and (d) 10 minutes.

Table 2 Particle size distributions of Ag-AuNPs and hot spot sizes of heterostructures

Incubation time (min)	Range of bimetallic particle size	Highest peak of particle size	Range of hot pot size	Highest peak of hot spot size
4	7.5-100 nm	8.5-115 nm	5.5-80 nm	7.5-90 nm
6	22 nm with a percentage of 34%	8.5 nm with a percentage of 38%	5.5 nm with a percentage of 38%	7.5 nm with a percentage of 16%
8	10-40 nm	3.5-17 nm	3-8.5 nm	6.3-15 nm
10	10 nm with a percentage of 47%	3.5 nm with a percentage of 37%	3 nm with a percentage of 73%	6.3 nm with a percentage of 43%

Figure 7(a–d) depicts EDS analysis of the Au and Ag nanoparticles which are deposited on textured Si, indicating the effective formation of bimetallic alloy Ag-AuNPs. The density of the AuNPs is lower than the AgNPs in the resulting bimetallic alloy Ag-AuNPs. This occurs because the deposition rate of AuNPs is lower than that of AgNPs since AuNPs need three electrons, while AgNPs requires only one electron, as presented in Eqs. (1) and (2) [19, 20].

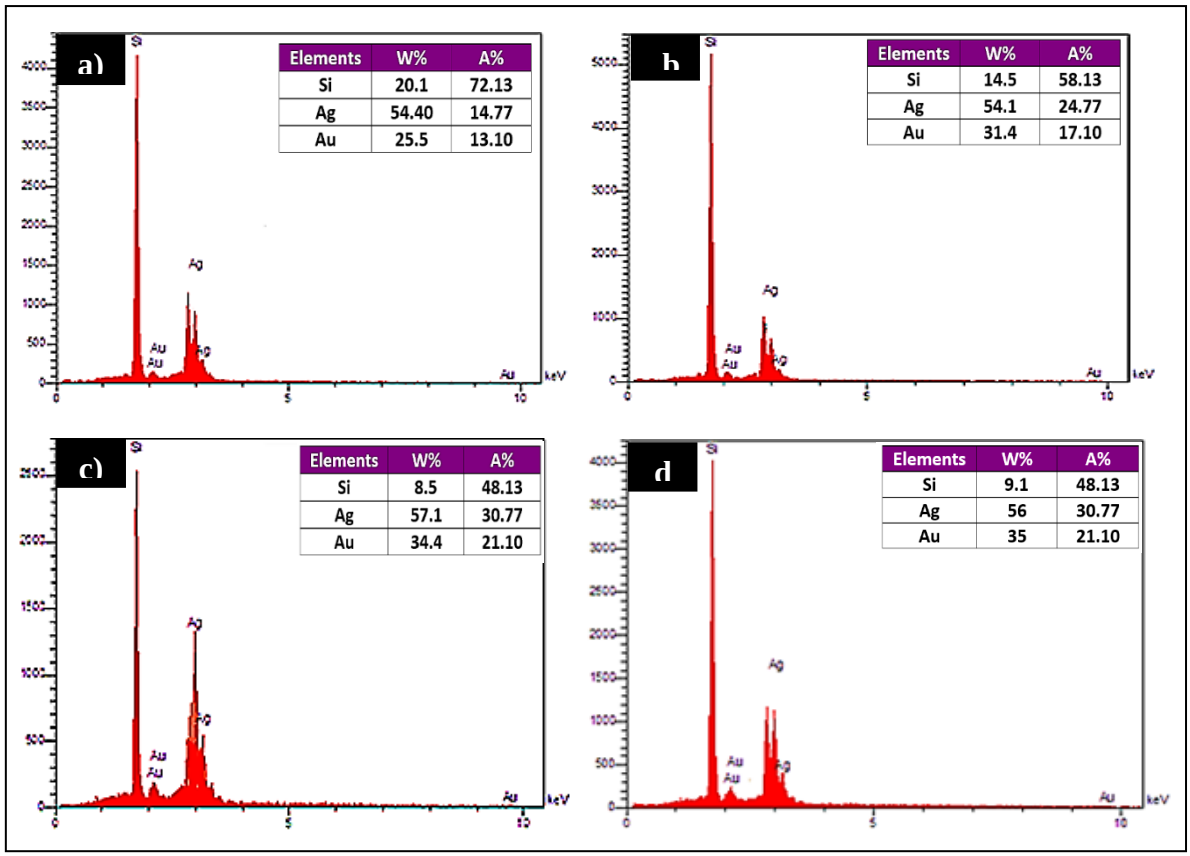

Figure 7. EDS analysis of Ag-AuNPs/nano hillocks Si SERS heterostructures at incubation time (a) 4 minutes, (b) 6 minutes, (c) 8 minutes, and (d) 10 minutes.

Figure 8(a–d) illustrates the XRD peaks of the Ag-AuNPs. There are two particular diffraction peaks at 38.3 A° and 44.5 A°. These two peaks are situated between gold peaks (ASTM card) and silver peaks (ASTM card) at phase indexes (1 1 1) and (2 0 0) of the face-centred cubic Ag-AuNPs. The resulting peaks of the bimetallic nanoparticles are broader than those of individually monometallic AuNPs and AgNPs [9]. These peaks can be supposed to overlap the individual diffraction peaks of Au and Ag nanoparticles [17]. The development of the bimetallic nanoparticles is due to the matching of the lattice parameters for gold and silver, which are 0.407 Å and 0.408 Å, respectively. This small variation in the lattice parameters is less than the thermal vibrations of the atoms and was assumed to allow alloy realization, even in nanometre regime [19].

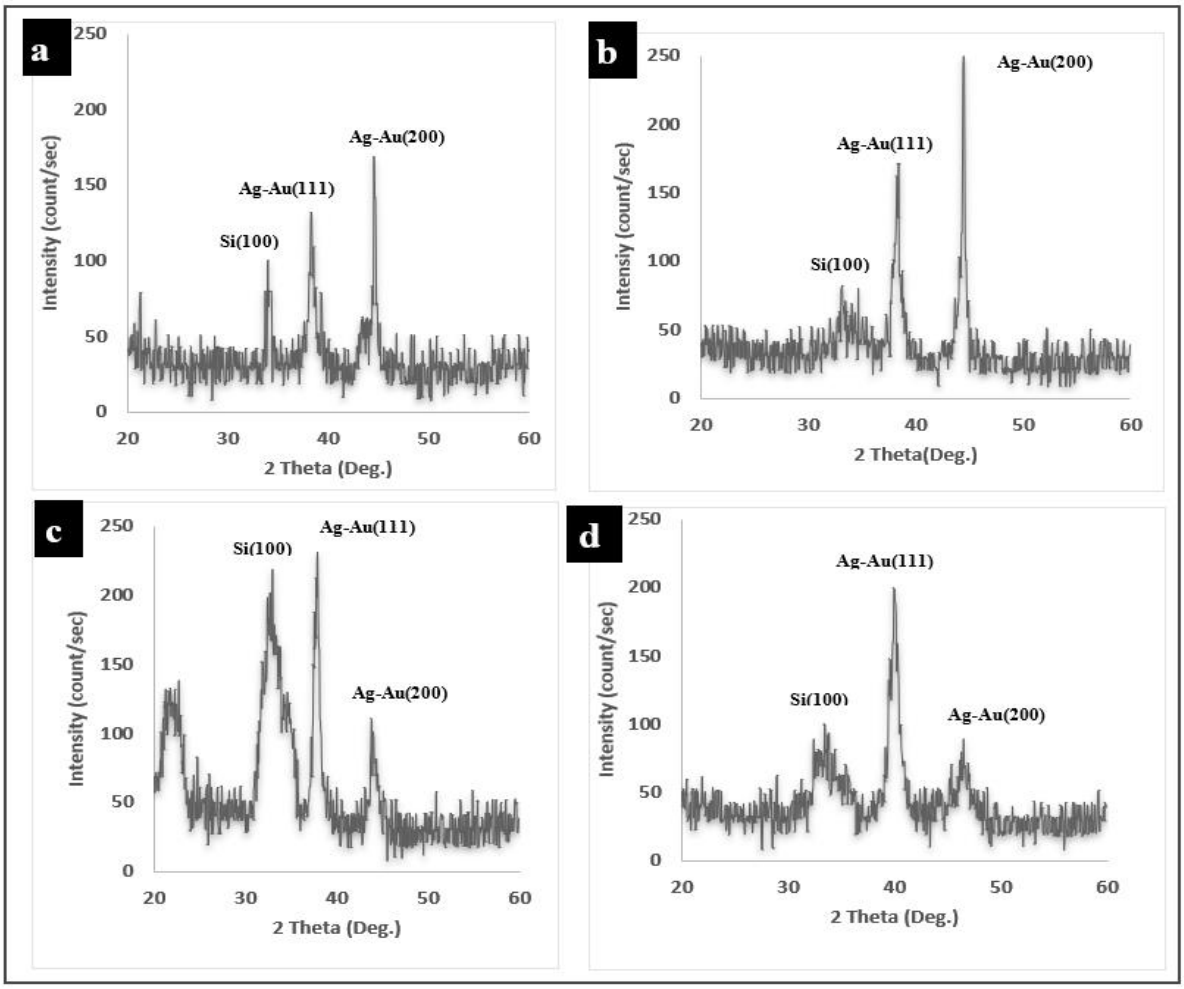

Figure 8. XRD pattern of the Ag-AuNPs incubation time (a) 4 minutes, (b) 6 minutes, (c) 8 minutes, and (d) 10 minutes.

The XRD data for the Ag-AuNPs are presented in Table (3). The difference in (2θ) is due to the formation of microscopic deformations (strain) and overlay of diffraction peaks [3]. The dependence of the bimetallic alloy and specific surface area (S.S.A.) of Ag-AuNPs on the incubation time shows specific aspects governing the properties of the bimetallic nanoparticles. The width of the diffraction peak is related to crystallite sizes, where higher crystallite sizes lead to sharp peaks and smaller sizes lead to broader peaks [21]. The observed broad peaks indicate rather small particle sizes and large S.S.A. values. The average bimetallic alloy Ag–Au NP grain size has been computed by utilizing Scherer's equation [21].

Table 3. Experimental and typical angles of diffraction (2θ) of Ag-AuNPs in the planes (111) and (200).

Incubation time(min)	2θ in (111) plane standard=38.3 experimental	2θ in (200) plane standard=44.5 experimental
4	38.3	44.5
6	38.4	44.4
8	38.1	43.8
10	39.9	46.5

The specific surface area (m^2/g) of the nanostructured material was computed by [3]:

$$S.S.A = \frac{6\times10^3}{G*\rho_{Ag-AuNPs}} \quad (3)$$

where G is the average grain size of the bimetallic alloy Ag-AuNPs (nm) and $\rho_{Ag-AuNPs}$ is the density of Ag-AuNPs (g/cm^3) that may be computed utilizing the following equation [21]:

$$\rho_{Ag-AuNPs} = \frac{i*\rho_{Au}+j*\rho_{Ag}}{i+j} \quad (4)$$

where i is the weight percentage of gold, j is the weight percentage of silver, and ρ_{Au} and ρ_{Ag} are the densities of gold (19.30 g/cm^3) and silver (10.50 g/cm^3), respectively. The values calculated for $\rho_{Ag-AuNPs}$ are 12.624, 11.943, 12.049, and 12.171 g/cm^3 for incubation times of 4, 6, 8, and 10 minutes, respectively. The S.S.A. values are illustrated in Table (4). From this table, one can observe that the highest S.S.A. of the Ag-AuNPs is about 92.9 (m^2/g) and was obtained for the 8 minutes incubation time.

Table 4 The average Ag-AuNPs grain size and S.S.A of the crystal plane (111)

Incubation time (min)	Nanoparticles(nm)	S.S.A.(m^2/g)
4	8.2	45
6	5.7	21.5
8	3.3	92.9
10	9.2	55.1

3.3 SERS Features Of Ag-Aunps/Nanohillocks Si SERS Heterostructures

To evaluate the SERS of the heterostructures, rhodamine 6G was selected as the target molecule. The heterostructures were immersed in R6G at concentrations of 10^{-8}, 10^{-10},10^{-12} and 10^{-14} M, and the as-prepared nanohillock Si substrate was tested at 10^{-4} M. Figure 9 shows that the R6G Raman spectrum for the nanohillock Si (without the bimetallic nanoparticles) presents a very small Raman signal with a specific peak located at 1647.8 cm^{-1}. Figure 10 depicts the SERS of SERS heterostructures as a function of incubation times. Five specific peaks of the Raman bonds are recorded in the range from 600-1600 cm^{-1}, at 1647.8, 1578, 1513, 1365 and 1230 cm^{-1}. These peaks are strongly connected to C–C and C–H bond stretching vibrations.

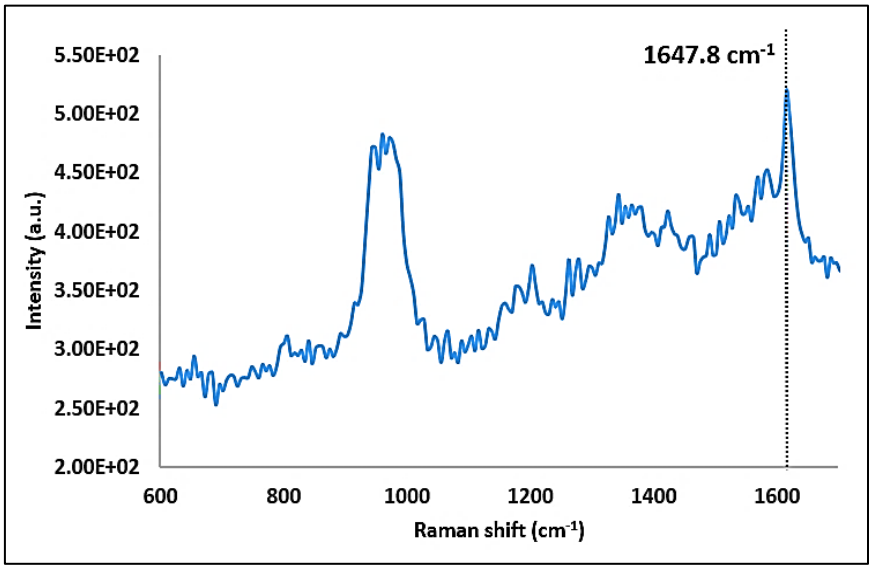

Figure 9. R6G Raman spectrum of as-prepared nano hillocks Si with 10^{-4}M concentration.

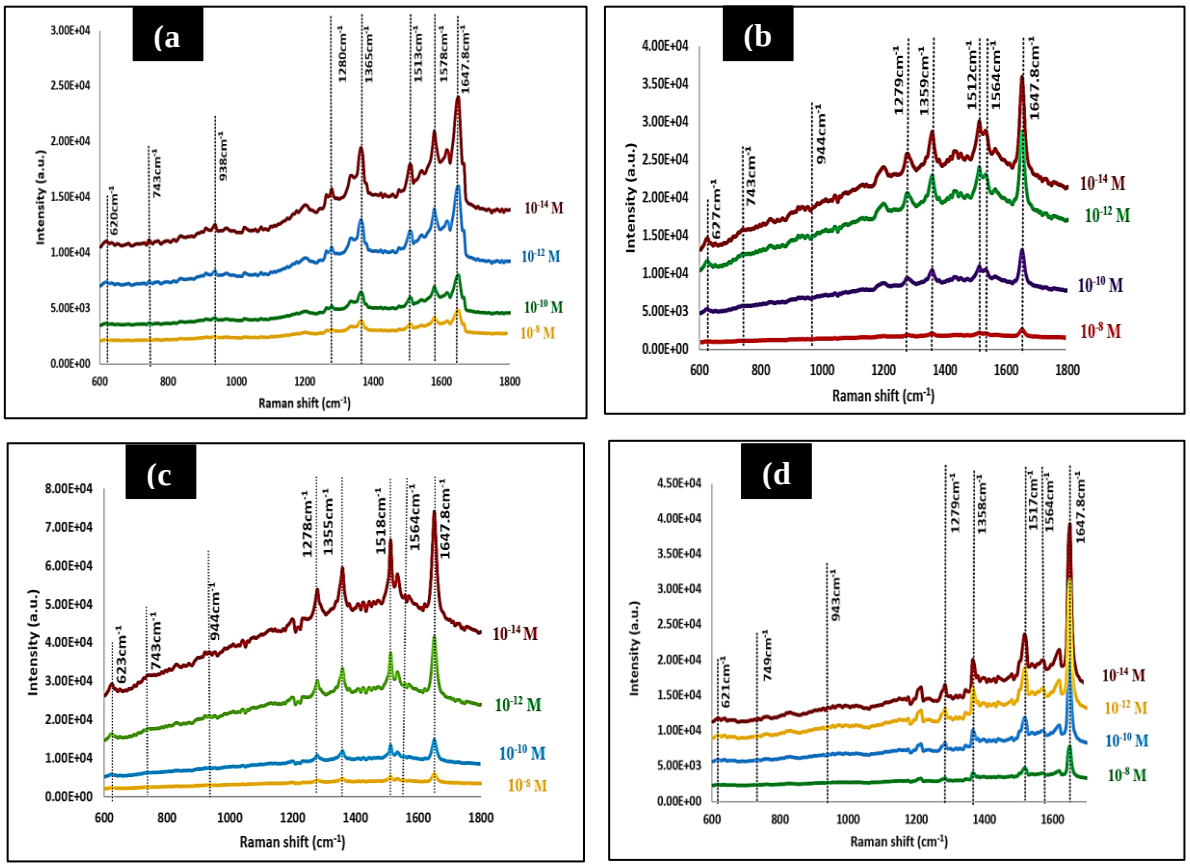

Figure 10. SERS spectra of Ag-AuNPs /nano hillocks Si SERS hetero strictures at concentrations 10^{-8}, 10^{-10}, 10^{-12} and 10^{-14} M of substrate prepared with incubation time (a) 4 minutes, (b) 6 minutes, (c) 8 minutes, and (d) 10 minutes.

Figure 11 demonstrates the variations in Raman peak intensity as a function of the incubation time. From this figure, one can note the increase in the Raman intensity with increasing incubation time from 4 to 8 minutes, while further increasing the incubation time to 10 minutes resulted in decreasing the intensity. This emphasizes the important effect of the incubation time on the performance of the SERS heterostructures. Adjusting the incubation times can be used to optimize both the surface roughness and the nanohillock height and hence the plasmonic characteristics of the Ag-AuNPs/nanohillocks Si SERS heterostructures.

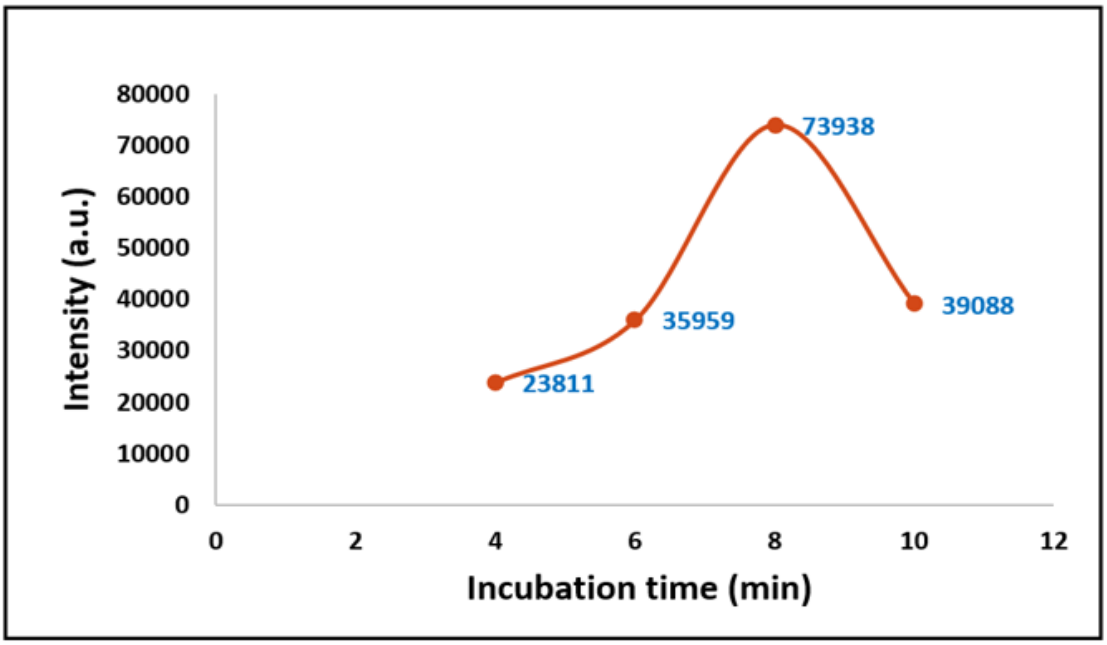

Figure 11. The variations of Raman peak intensity of the R6G at 1647.8 cm^{-1} with incubation time.

The enhancement factor (EF) of Raman signal intensity is computed by the following equation [2]:

$$EF = \frac{I_{SERS}/C_{SERS}}{I_{RS}/C_{RS}} \quad (5)$$

where I_{SERS} is the SERS signal of the heterostructures at a particular concentration of C_{SERS} and I_{RS} is the Raman signal of the Si nanohillocks with a concentration of C_{RS}.

The highest Raman peak at 1647.8 cm^{-1} was used as a reference peak in calculating the EF of the heterostructures. The values of the EF at different concentrations are listed in Table (5). At the lowest concentration, 10^{-14} M, the highest EF of the Raman signal was obtained for heterostructures with an 8 minutes incubation time resulting in a value of 3.7×10^{13}. In contrast, the lowest EF, 5×10^{10}, was obtained for the heterostructures with a 4 minutes incubation time. This large variation in EF (three orders of magnitude) is related to the topographical features (surface roughness and pyramid height) of the textured silicon and hence the plasmonic characteristics (due to hot spots and isolated Ag-AuNPs) of the Ag-Au nanoparticle heterostructures. The histogram of the plasmonic characteristics is presented in Figure 6(a-d) and Table (2). The lowest EF was for heterostructures with a 4 minutes incubation time. These aggregated bimetallic nanoparticles had a large size (22 nm) and covered 34% of the surface, while the nano-gaps were 10 nm in size and covered 47% of the surface, resulting in very little influence on the Raman intensity enhancement. This case had the lowest EF value as a result of the low percentage of hot spot regions and the existence of passive bimetallic nano-particle regions.

The highest EF was for heterostructures with 8 minutes incubation time. These aggregated bimetallic nanoparticles had a small size (3 nm) and covered 73% of the surface, while the nano-gaps were 5.5 nm in size and covered 38% of the surface, as shown in Table (2).

The dependence of the Raman EF on the Ag-AuNP sizes can be understood in terms of the S.S.A. of the Ag-AuNPs, as indicated in Table (5). The improvement of S.S.A. can contribute to a large magnitude of the effective energy transfer within the hot spot matrix [9].

Table 5 The values of the enhancement factor of heterostructures

R6G concentration(m)	EF 4 min	EF 6 min	EF 8 min	EF 10 min
10^{-8}	4.4×10^{5}	7.5×10^{5}	7.4×10^{8}	9.2×10^{4}
10^{-10}	6.9×10^{7}	6×10^{7}	3.7×10^{10}	1.5×10^{7}
10^{-12}	2.5×10^{9}	3.8×10^{9}	1.5×10^{12}	3.1×10^{9}
10^{-14}	5×10^{10}	1.5×10^{11}	3.7×10^{13}	4.6×10^{11}

The reproducibility of the SERS spectra for the heterostructure substrate using 8 minutes incubation time due to its higher EF was studied for 10 batches. Figure 12(a) presents the intensity spectra. The alteration in the SERS intensity of the highest Raman peak, 1647.8 cm^{-1}, is shown in Figure 12(b). Excellent reproducibility (variations down to 4%) was recorded for the heterostructure substrate. The main reason for this well-organized performance is due to the uniformity of the surface morphology of Ag-AuNPs/nanohillocks Si SERS heterostructures, as well as the size distribution of the Ag-AuNPs on the textured silicon. This low value of variation and high reproducibility on both the microscopic and macroscopic scale is because of the high degree of surface uniformity after the deposition of bimetallic nanoparticles. The clarification of the above statement is reinforced by the measured morphological properties of the resulting heterostructure.

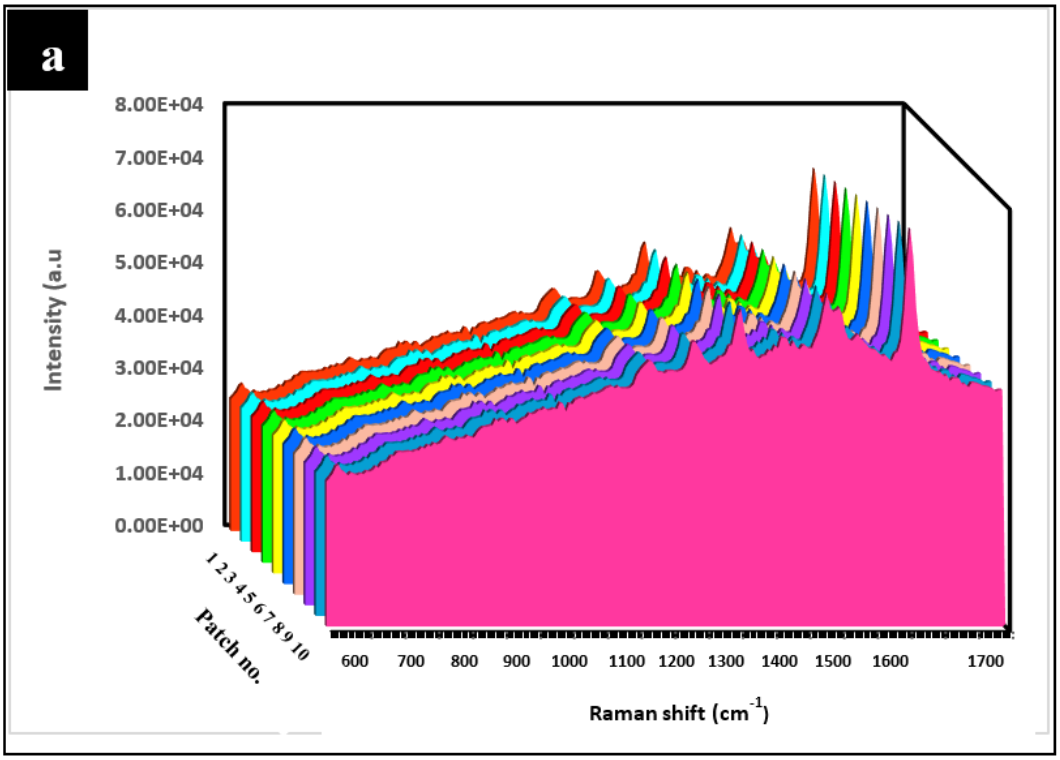

Figure 12. (a) SERS spectrum reproducibility of SERS signal.

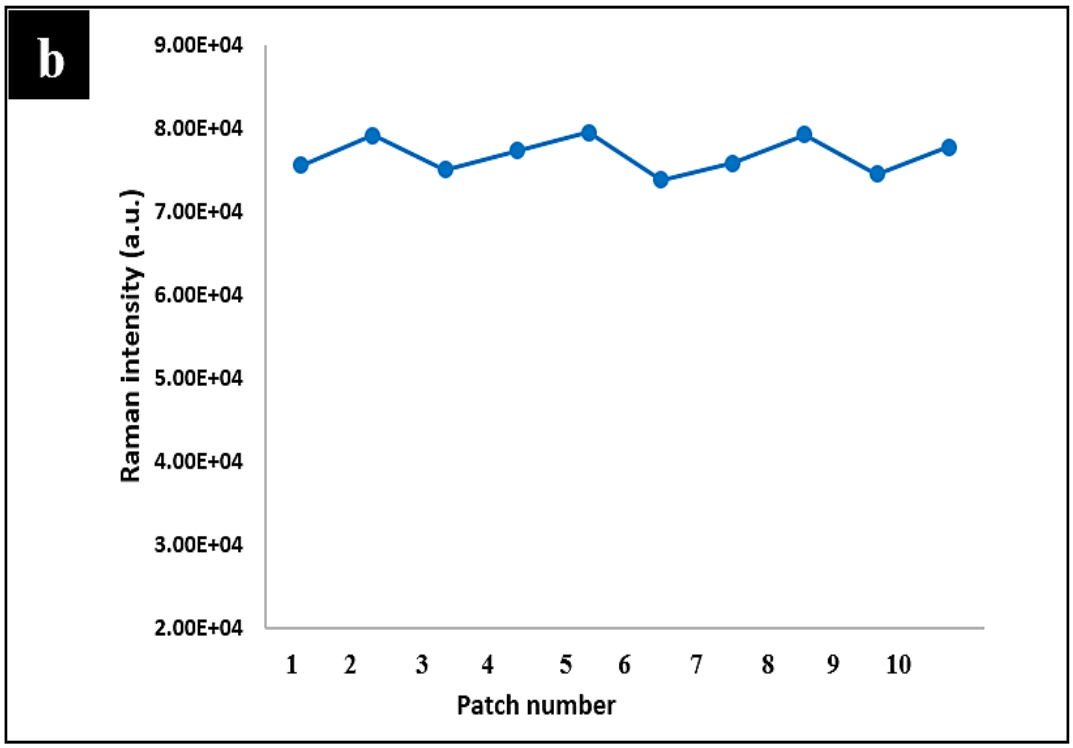

Figure 12. (b) The reproducibility of Raman peak 1647.8cm^{-1} of 10^{-14} M.

4. CONCLUSION

In this work, the Raman spectra of Ag-AuNPs/nanohillocks Si SERS heterostructures for R6G detection was efficiently improved. The heterostructures were synthesized and optimized based on textured single-crystal Si by controlling the bimetallic Ag-AuNP sizes and hot spot regions. Good control of the topographical features of textured silicon (surface roughness, surface skewness and average hillock height) by incubation time led to the synthesis of various types of bimetallic SERS heterostructures. The SERS performance of the heterostructures was assessed for a very low concentration, 10^{-14} M, of R6G dye. The SERS performance of heterostructures increased with increasing surface roughness, surface skewness and average nanohillock height. The supreme performance of these Ag-AuNPs/nanohillocks Si SERS heterostructures introduces a novel approach for highly sensitive SERS detection of biomolecules.

ACKNOWLEDGEMENTS

Authors would like to express gratitude to the Department of Applied Sciences/University of Technology for assistance with the preparation of the samples.

REFERENCES

[1] Li, Zhe, S. C., Zhang, C., Liu, X. Y., Gao, S. S., Hu, L. T., ... & Si, H. P. "High-performance SERS substrate based on hybrid structure of graphene oxide/AgNPs/Cu film@ pyramid Si." Scientific Reports 6 (2016) 38539.

[2] Jabbar, Allaa A., Alwan M. Alwan, & Adawiya J. Haider. "Modifying and fine controlling of silver nanoparticle nucleation sites and SERS performance by a double silicon etching process." Plasmonics 13.4 (2018) 1171-1182.

[3] A. M. Alwan, L. A. Wali & A. A. Yousif, Optimization of AgNPs/mesoPS active substrates for ultra-low molecule detection process, Silicon 10 (2018) 2241-2251.
[4] Zhang, C., Man, B. Y., Jiang, S. Z., Yang, C., Liu, M., Chen, C. S., ... & Li, Z. "SERS detection of low-concentration adenosine by silver nanoparticles on silicon nanoporous pyramid arrays structure." Applied Surface Science **347** (2015) 668-672.
[5] Bandarenka, H., Girel, K., Zavatski, S., Panarin, A., & Terekhov, S. "Progress in the development of SERS-active substrates based on metal-coated porous silicon." Materials **11.5** (2018) 852.
[6] Mosier-Boss, Pamela. "Review of SERS substrates for chemical sensing." Nanomaterials **7.6** (2017) 142.
[7] Khaywah, M. Y., Jradi, S., Louarn, G., Lacroute, Y., Toufaily, J., Hamieh, T., & Adam, P. M. "Ultrastable, uniform, reproducible, and highly sensitive bimetallic nanoparticles as reliable large scale SERS substrates." The Journal of Physical Chemistry C **119.46** (2015) 26091-26100.
[8] Alwan, Alwan M., Muslim F. Jawad, & Duaa A. Hashim. "Enhanced Morphological Properties of Macroporous Silicon with the Incorporation of Au-Ag Bimetallic Nanoparticles for Improved CO2 Gas Sensing." Plasmonics, (2019) 1-11.
[9] Wali, Layla A., Khulood K. Hasan, & Alwan M. Alwan. "Rapid and highly efficient detection of ultra-low concentration of Penicillin G by gold nanoparticles/porous silicon SERS active substrate." Spectrochimica Acta Part A: Molecular and Biomolecular Spectroscopy **206** (2019) 31-36.
[10] Wang, F., Zhang, X., Wang, L., Jiang, Y., Wei, C., & Zhao, Y. "Pyramidal texturing of silicon surface via inorganic-organic hybrid alkaline liquor for heterojunction solar cells." Journal of Power Sources **293** (2015) 698-705.
[11] Khanna, A., Basu, P. K., Filipovic, A., Shanmugam, V., Schmiga, C., Aberle, A. G., & Mueller, T. "Influence of random pyramid surface texture on silver screen-printed contact formation for monocrystalline silicon wafer solar cells." Solar Energy Materials and Solar Cells **132** (2015) 589-596.
[12] Haiss, W., Raisch, P., Bitsch, L., Nichols, R. J., Xia, X., Kelly, J. J., & Schiffrin, D. J. "Surface termination and hydrogen bubble adhesion on Si (1 0 0) surfaces during anisotropic dissolution in aqueous KOH." Journal of Electroanalytical Chemistry **597.1** (2006) 1-12.
[13] Zhuang, D., & J. H. Edgar. "Wet etching of GaN, AlN, and SiC: a review." Materials Science and Engineering: R: Reports **48.1** (2005) 1-46.
[14] Kim, J., Inns, D., Fogel, K., & Sadana, D. K. "Surface texturing of single-crystalline silicon solar cells using low density SiO2 films as an anisotropic etch mask." Solar Energy Materials and Solar Cells **94.12** (2010) 2091-2093.
[15] Seidel, H., Csepregi, L., Heuberger, A., & Baumgärtel, H."Anisotropic etching of crystalline silicon in alkaline solutions I. Orientation dependence and behavior of passivation layers." Journal of the electrochemical society **137.11** (1990) 3612-3626.
[16] Allongue, Philippe, Virginia Costa-Kieling, and Heinz Gerischer. "Incubationing of Silicon in NaOH Solutions II. Electrochemical Studies of n-Si (111) and (100) and Mechanism of the Dissolution." Journal of the Electrochemical Society **140.4** (1993) 1018-1026.
[17] Gosálvez, M. A., *et al.* "An atomistic introduction to anisotropic etching." Journal of Micromechanics and Microengineering **17.4** (2007) S1.
[18] Sana, P., Vázquez, L., Cuerno, R., & Sarkar, S. "Collective evolution of submicron hillocks during the early stages of anisotropic alkaline wet chemical incubationing of Si (100) surfaces." Journal of Physics D: Applied Physics **50.43** (2017) 435306.
[19] Wali, L. A., Alwan, A. M., Dheyab, A. B., & Hashim, D. A. "Excellent fabrication of Pd-Ag NPs/PSi photocatalyst based on bimetallic nanoparticles for improving methylene blue photocatalytic degradation." Optik **179** (2019) 708-717.
[20] Jabbar, Allaa A., & Alwan M. Alwan. "Efficient detecting of TNT molecules using Palladium nanoparticles/cross shape pores like structure porous silicon." Vibrational Spectroscopy, (2019) 102933.

[21] Duaa A. Hashim, Alwan M. Alwan1 & Muslim F. Jawad, "An investigation of Structural Properties of Monometallic (Ag, Pd) and Bimetallic (Ag@Pd) Nanoparticles Growth on Macro Porous Silicon ", International Journal of Nanoelectronics and Materials **11**, 4 (Oct 2018)**.**